

# A SEMI-EMPIRICAL SYNTHESIS OF ROBUST FEEDBACKS USING $\mu$ -MANIFOLDS

Boe-Shong Hong and Qing-Zhou Huang

*Department of Mechanical Engineering, National Chung Cheng University*

## ABSTRACT

This paper prospects the topology of a class of robust feedbacks measured by structured singular value. It starts at delimiting the full extent of frequency domain in searching for a feasible system characterized by performance-in-specification, reliability-in-operation and order-of-compensator. This makes possible extension of the design-test-analysis approach that is popular in industry to a semi-empirical synthesis to shorten the time consumed in controller development. The research journey ends at an illustrated example where the prospected topology is used to develop robust loop-filters in phase-lock-loop circuits served for frequency-to-voltage transducers.

**Keywords:** robust control, semi-empirical synthesis, phase-lock loop circuit

## 以結構化奇異值為尺度之半經驗式矯健迴授設計

洪博雄 黃慶洲

中正大學機械工程學系

## 摘要

本文探勘一些以結構奇異值為尺度的矯健迴授系統之拓樸。首先在頻域裡，圖解出所有合用之閉迴路所在區域，而以需求之性能，運作可靠度與補償器階數，對合用區域內每一個成員作一綜合評價。借此工具，實務界常用之設計-測試-分析方法可延伸為半經驗控制器合成法，以縮短開發時間。最後，本文以開發用於頻壓轉換之相鎖迴路濾波器為例，說明此拓樸工具的用法。

**關鍵詞：**矯健控制，半經驗迴授合成，相鎖迴路

## I. INTRODUCTION

This article concerns a class of feedback compensations that possesses the following attributes:

- (A1) The plant is of single input and single output, which is with a feedback compensator to track a single command.
- (A2) The feedback compensator can be implemented, passively or actively, into an analog circuit.
- (A3) The nominal plant's model is appointed with low-order and time-invariant linearity.
- (A4) Perturbations of the nominal model are lumped by a multiplicative uncertainty, bounded by  $H_\infty$ -norm, in frequency domain.
- (A5) Performance of the closed-loop is specified in time domain by the induced  $L_2$ -norm from the command to the tracking error.

For achieving robust compensators that suit (A1)-(A5), analytic approaches such as LFT- $H_\infty$  synthesis [1], LMIs-based synthesis [2-3] and observer-based  $L_2$ -gain synthesis [4-5] are popular in academia. However, they formulate the set of compensators of orders merely close to that of the generalized plant, which implicates the situation of either order-overabundance in that feasible compensators exist in much lower orders or order-shortage in that candidate compensators only exist in higher orders. We hereof provide a topological tool that graphs all orders of feasible closed-loops as a nonparametric set in the complex domain, named by  $\mu$ -manifold, for checking whether an order-ill-devised compensator has been calculated out of one of these analytic synthesizers. This topological tool is in aid of the forward compensation of the generalized plant [6] and order truncation of feedback compensator [7] for seeking an order-well-devised feedback compensator, which, due to page limit, is beyond the focus of this article.

On the other hand, most of feedback compensators in industry are empirically hunted out of the iteration of design-test-analysis in

frequency domain. This is a straightforward way of achieving a compensator with candidacy judged by the performance-in-specification (PS) and reliability-in-operation (RO) of the closed loop as well as the order of compensator (OC). Since the  $\mu$ -manifold delimits the full extent in searching for feasible compensators, to study a (PS, OC, and RO)-characterized  $\mu$ -manifold's topology ( $\mu$ -topology) is in demand for a fully custom-made compensator. Empirical approaches with the  $\mu$ -topology extend for a semi-empirical synthesis that reduces both the time consumed in the process of iteration and the conservatism in setting up specifications for the associated product, and then strengthens marketing competition.

Three sections present the development of the  $\mu$ -topology. Section 3 measures with structured singular value ( $\mu$ ) the robust performance of systems attributed to (A1)-(A5). It is unnecessary for readers to have known  $\mu$ -synthesis in advance. Section 4 develops the topology of  $\mu$ -measured systems to explore the trade-offs among PS, RO and OC, based on which a semi-empirical synthesizer is proposed. Section 5 applies the  $\mu$ -topology-aided synthesis to loop filtering of phase-lock-loop (PLL) circuits served for frequency-to-voltage transducers. This application can be treated as an instruction in putting the  $\mu$ -topology into use.

## II. MATHEMATICAL PRELIMINARIES

Mathematical notation of this article is as follows. For a dynamical system  $G$ , the symbol  $G$  itself is used as shorthand for its transfer function  $G: C \rightarrow C$ . When a fixed frequency  $\omega$  is signified, the symbol  $G$  is further used as shorthand for the complex value  $G(j\omega)$ . For a signal  $z$ ,  $z(t)$  denotes its real value in time domain at time  $t$  and  $z(j\omega)$  denotes its complex value in frequency domain at frequency  $\omega$ , where

$$z(j\omega) \equiv \frac{1}{\sqrt{2\pi}} \int_0^\infty z(t)e^{-j\omega t} dt, \quad \omega \in (-\infty, \infty);$$

$$z(t) \equiv \frac{1}{\sqrt{2\pi}} \int_{-\infty}^{\infty} z(j\omega) e^{j\omega t} d\omega, \quad t \in [0, \infty).$$

The  $L_2$ -norm of the signal  $z$ ,  $\|z\|_{L_2}$ , is defined by

$$\|z\|_{L_2}^2 \equiv \int_0^{\infty} \|z(t)\|^2 dt,$$

where  $\|\cdot\|$  denotes the Euclidean norm of a finite-dimensional vector, and its  $H_2$ -norm,  $\|z\|_{H_2}$ , is defined by

$$\|z\|_{H_2}^2 \equiv \int_{-\infty}^{\infty} \|z(j\omega)\|^2 d\omega.$$

Suppose the system  $G$  has the input signal  $w$  and output signal  $z$ , then the induced  $L_2$ -norm ( $L_2$ -gain) of the system  $G$ ,  $\|G\|_{L_2 \rightarrow L_2}$ , is defined by

$$\|G\|_{L_2 \rightarrow L_2} \equiv \sup_w \frac{\|z\|_{L_2}}{\|w\|_{L_2}},$$

and its  $H_\infty$ -norm,  $\|G\|_\infty$ , is defined by

$$\|G\|_\infty \equiv \sup_w \frac{\|z\|_{H_2}}{\|w\|_{H_2}}.$$

Based on the geometrical isomorphism between time domain and frequency domain [8],  $H_2$ -norm and  $H_\infty$ -norm are identical to  $L_2$ -norm and  $L_2$ -gain, respectively, that is,

$$\|z\|_{L_2} = \|z\|_{H_2} \equiv \|z\|_2; \quad \|G\|_\infty = \|G\|_{L_2 \rightarrow L_2}.$$

### III. THE CLASS OF $\mu$ -MEASURED SYSTEMS

This section deduces the sufficient and necessary condition of robust performance for the class of systems attributed to (A1)-(A5). Figure 1 carries required reasoning.

The plant in the closed loop plotted in Figure 1a can be an arbitrary member of a dense set  $(G, W_1)$ ,

$$(G, W_1) \equiv \{G(1 + \Delta_1 W_1) : \|\Delta_1\|_\infty \leq 1\}, \quad (1)$$

where  $G$  is the nominal plant and  $W_1$  is a robustness weighting. With a magnitude scaling

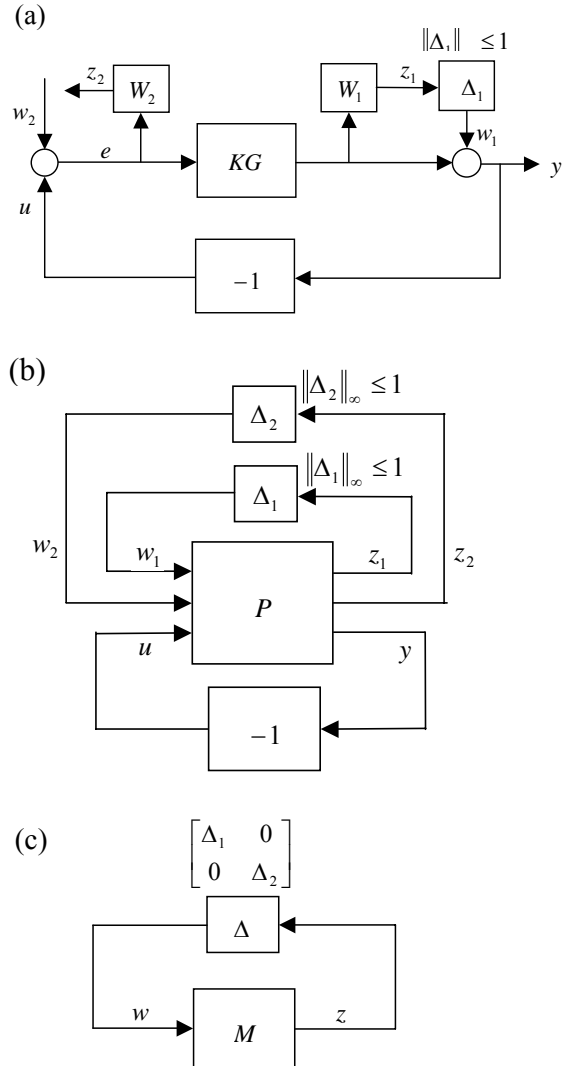


Fig.1. (a) Closed-loop demanding for robust performance, (b) Robust stability of Figure 1a, (c) Fractional transformation of Figure 1b.

$\Delta_1$  bounded by  $H_\infty$ -norm, i.e.  $|\Delta_1(j\omega)| \leq 1$  for all  $\omega$ , the complex value  $W_1(j\omega)$  indicates length and phase of the multiplicative uncertainty  $\Delta_1 W_1$  at frequency  $\omega$ . The compensator  $K$ , pre- or post- composite to the plant, together with a negative unit feedback  $-1$  executes the feedback compensation. Under the model uncertainty  $\Delta_1 W_1$  and exogenous input  $w_2$ , which is a combination of referenced command and plant disturbance, the  $L_2$ -gain performance is specified by

$$\|z_2\|_{L_2}^2 < \|w_2\|_{L_2}^2, \forall w_2 \in L_2[0, \infty), \quad (2)$$

where  $z_2$  is a weighted tracking error obtained by putting a performance weighting  $W_2$  on the tracking error  $e$ , i. e.  $z_2(j\omega) = W_2(j\omega)e(j\omega)$  for all  $\omega$ .

**Definition 1 (feasible loop):** Regarding to Figure 1a, a feasible loop is one of those sensitivity functions,  $S = 1/(1 + KG)$ , that guarantee  $L_2$ -gain performance of Eq. (2) for all plants in  $(G, W_1)$ . Any feasible loop corresponds to a system of *robust performance*.

◆

Tracing the path of signal flow in Figure 1a can equally render the system of Figure 1a into one with three feedback-coupled subsystems, which are

Generalized plant:

$$\begin{bmatrix} z_1 \\ z_2 \\ y \end{bmatrix} = \begin{bmatrix} 0 & W_1 KG & W_1 KG \\ 0 & W_2 & W_2 \\ 1 & KG & KG \end{bmatrix} \begin{bmatrix} w_1 \\ w_2 \\ u \end{bmatrix}; \quad (3)$$

External feedback:

$$u = -y; \quad (4)$$

Internal feedback 1:

$$w_1 = \Delta_1 z_1, \|\Delta_1\|_\infty \leq 1. \quad (5)$$

The system of Figure 1b consists of a supplementary subsystem to Eqs. (3)-(5),

Internal feedback 2:

$$w_2 = \Delta_2 z_2, \|\Delta_2\|_\infty \leq 1. \quad (6)$$

Due to this artificial feedback, the robust performance of the system of Figure 1a is equivalent to the robust stability of the system of Figure 1b, that is, the guarantee of stability for uncertainties  $\Delta_1$  and  $\Delta_2$  bounded by

$\|\Delta_1\|_\infty \leq 1$  and  $\|\Delta_2\|_\infty \leq 1$ . This equivalence has a simple rationale explained as follows. Since  $|\Delta_2(j\omega)| \leq 1$  for all  $\omega$ , based on Nyquist criterion the robust stability of Figure 1b requires that in the absence of  $\Delta_2$ , for all  $\omega$ ,  $z_2(j\omega)/w_2(j\omega)$  be a point inside the unit circle centered at the origin, for all  $\|\Delta_1\|_\infty \leq 1$ . In other words, for all  $\|\Delta_1\|_\infty \leq 1$  the  $H_\infty$  norm of the transfer function  $z_2/w_2$  in Figure 1a has to be smaller than 1, that is, the  $L_2$ -gain is smaller than 1 as described in Eq. (2), and then the robust performance of Figure 1a is true. Reversing the deduction above can directly draw the inverse inference that robust performance of Figure 1b implies robust stability of Figure 1a.

The system of Figure 1c is obtained from the Figure 1b via substituting the external feedback in Eq. (4) into the generalized plant in Eq. (3) as well as stacking the two internal feedbacks in Eq. (5) and Eq. (6). An according calculation yields

$$M = \begin{bmatrix} -W_1 T & W_1 T \\ -W_2 S & W_2 S \end{bmatrix}, \quad \Delta = \begin{bmatrix} \Delta_1 & 0 \\ 0 & \Delta_2 \end{bmatrix}, \quad (7)$$

$$z = \begin{bmatrix} z_1 \\ z_2 \end{bmatrix}, \quad w = \begin{bmatrix} w_1 \\ w_2 \end{bmatrix},$$

where  $S$  is the sensitivity function  $1/(1 + KG)$  and  $T$  is its complementary function, i. e.  $S + T = 1$ . If the  $\Delta$ -structured singular value  $\mu_\Delta : C^{2 \times 2} \rightarrow R^+ \cup \{0\}$  for a fixed frequency  $\omega$  is defined by

$$\mu_\Delta(M) = \frac{1}{\min\{\bar{\sigma}(\Delta) : \det(I - M\Delta) = 0\}}, \quad (8)$$

where  $\bar{\sigma}(\Delta)$  denotes the maximum singular value of the matrix  $\Delta$ , then based on the Nyquist criterion the stability of Figure 1c is guaranteed if and only if

$$\mu_\Delta(M(j\omega)) \leq 1, \forall \omega. \quad (9)$$

This conclusion could be referred to [9]. Substituting Eq. (7) into Eq. (8) yields

$$\mu_{\Delta}(M) = \frac{1}{\min\{\max(|\Delta_1|, |\Delta_2|) : 1 + W_1 T \Delta_1 - W_2 S \Delta_2 = 0\}} \quad (10)$$

and further calculating results in

$$\mu_{\Delta}(M) = |W_1 T| + |W_2 S|. \quad (11)$$

Based on Eq. (11) and Eq. (9), the set of all feasible loops  $S$ 's is now known as

$$\left\{ \begin{array}{l} |S| : |W_1(j\omega)(1 - S(j\omega))| + |W_2(j\omega)S(j\omega)| \\ < 1, \forall \omega \end{array} \right\} \quad (12)$$

A graphical interpretation of robust performance is in Figure 2, where the line segment of  $S+T=1$  inside the diamond of  $\mu_{\Delta}(M)=1$  represents the set of all feasible loops. This figure also illustrates the conservatism of singular value  $\bar{\sigma}(M)$  and the risk of spectral radius  $\rho(M)$  as a metric of robust performance.

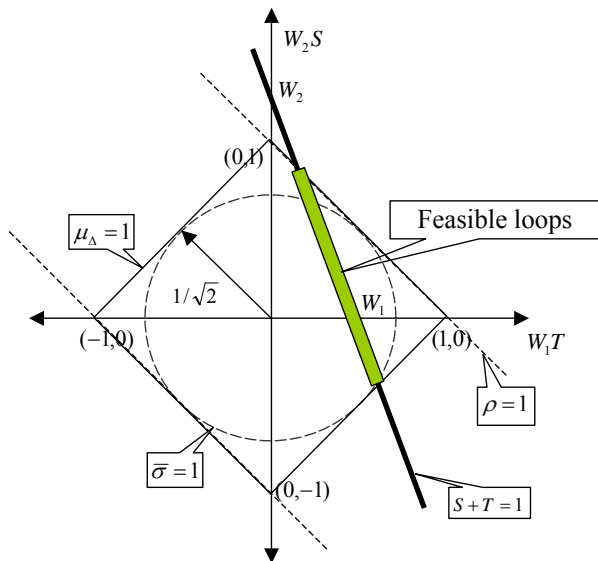


Fig.2. Graphical interpretation of robust performance.

## IV. THE $\mu$ -TOPOLOGY

**Definition 2 ( $\mu$ -plate and  $\mu$ -manifold):** At frequency  $\omega$ , the open, convex, complex-valued set  $\{S : |W_1(1-S)| + |W_2S| < 1\}$  maps a  $\mu$ -plate  $\beta_{\omega}(W_1, W_2)$  in the 2D plane Cartesian-coordinated by  $\text{Re}(S)$  and  $\text{Im}(S)$ . The 3D  $\mu$ -manifold  $\beta(W_1, W_2)$  is stacked up by  $\mu$ -plates  $\beta_{\omega}(W_1, W_2)$  along the longitudinal axis  $\omega$ .  $\blacklozenge$

There is one-to-one mapping between the set of feasible loops in Definition 1 and the set of longitudinal lines inside the  $\mu$ -manifold  $\beta(W_1, W_2)$  in Definition 2. Every compensator  $K$  of feasibility has to render that the sensitivity function  $S$ ,  $S = 1/(1 + KG)$ , maps a line inside the  $\mu$ -manifold.

As follows is given an account of geometrical properties of the  $\mu$ -plate  $\beta_{\omega}(W_1, W_2)$  with respect to the robustness weighting  $W_1$  and performance weighting  $W_2$  at every frequency  $\omega$ .

- (P1) Every  $\mu$ -plate is symmetric to the  $\text{Re}(S)$  axis.
- (P2) As  $|W_1|$  and  $|W_2|$  are both greater than 1, the  $\mu$ -plate is vanished.
- (P3) As  $|W_1| \geq |W_2|$  and not both of  $|W_1|$  and  $|W_2|$  are greater than 1, the  $\mu$ -plate is contained in an ellipse that has foci  $(0,0)$  and  $(1,0)$ , semimajor axis  $1/2|W_2|$ , and semiminor axis  $\sqrt{1 - |W_2|^2} / 2|W_2|$ .
- (P4) As  $|W_2| \geq |W_1|$  and not both of  $|W_1|$  and  $|W_2|$  are greater than 1, the  $\mu$ -plate is contained in an ellipse that has foci  $(0,0)$  and  $(1,0)$ , semimajor axis  $1/2|W_1|$ , and semiminor axis  $\sqrt{1 - |W_1|^2} / 2|W_1|$ .
- (P5) As  $|W_1| = |W_2| < 1$ , the boundary of the  $\mu$  plate is just the ellipse described in (P3) or (P4).
- (P6) As  $|W_1| = |W_2| \approx 1$ , the  $\mu$ -plate degenerates into a line segment between  $(0,0)$  and  $(1,0)$ .

(P7) As  $|W_1| \gg |W_2|$ , the boundary of  $\mu$ -plate is close to a circle of radius  $1/|W_1|$  centered at  $(1,0)$ .

(P8) As  $|W_2| \gg |W_1|$ , the boundary of  $\mu$ -plate is close to a circle of radius  $1/|W_2|$  centered at  $(0,0)$ .

These properties (P1)-(P8) about the  $\mu$ -plates are simply inherited from the characteristic dimension of an elliptical orbit with two specified focuses.

Several constitutional points regarding  $\mu$ -measured robust feedbacks can be inferred from (P1)-(P8). Firstly, a  $\mu$ -plate  $\beta_\omega(W_1, W_2)$  tends to disappearance with simultaneously magnified robustness weighting  $W_1$  and performance weighting  $W_2$ , which reveals the trade-off between robustness and performance. Secondly, if the uncertainty is distributed in high frequency and then obviously the transient response can't be guaranteed, then the performance weighting  $W_2$  allows only of low-pass filtering for stressing steady-state responses. This signifies that there is a trade-off between transient response and steady response. Finally, an increased action input to the plant, which is followed by a raised gain of compensator  $K$  that diminishes the sensitivity function  $S$ , reduces the tracking error  $e$ . This discloses a trade-off between control action and the tracking error. These trade-off natures have been commonly experienced in feedback-control engineering as in [10].

A closed-loop system can be custom-made according to a triad: performance-in-specification (PS), reliability-in-operation (RO) and order-of-compensator (OC). The PS is measured with areas of  $\mu$ -plates that are determined by the pair of robustness and performance weightings,  $(W_1, W_2)$ , as shown in (P1)-(P8). A wide (narrow)  $\mu$ -manifold  $\beta(W_1, W_2)$  corresponds to a low (high) performance in specification. The *reliability distance* that is defined in following measures the RO:

**Definition 3 (Reliability distance):** The *reliability distance*  $d: [0, \infty) \rightarrow R$  of a feasible

loop  $S$  is defined by that the real value  $d(\omega)$  at frequency  $\omega$  is the shortest distance between the boundary of the  $\mu$ -plate  $\beta_\omega(W_1, W_2)$  and the point where the longitudinal line of feasible loop  $S$  penetrates through the  $\mu$ -plate  $\beta_\omega(W_1, W_2)$ . ♦

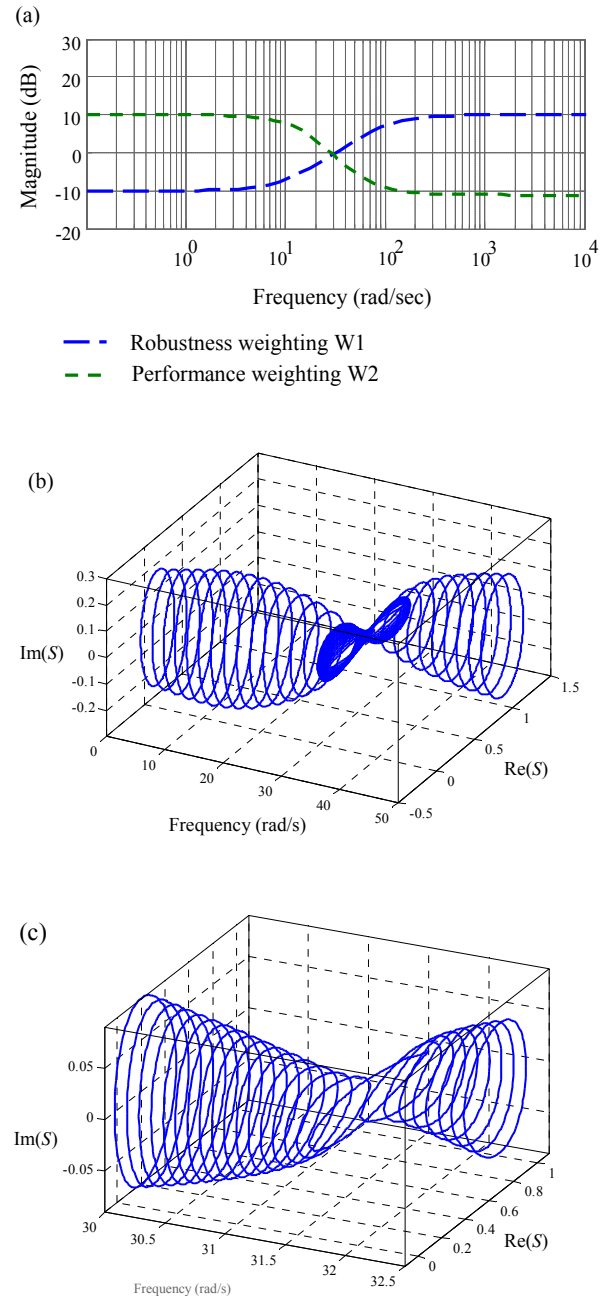


Fig.3. (a) Robustness and performance weightings of Example 1, (b) The  $\mu$ -manifold of Example 1, (c) Close view of Figure 3b.

The reliability distance  $d$  quantifies the capability of accommodating exceeded disturbances and modeling uncertainties in real operation. As for the OC, it affects the quality of real-time processing and the accuracy of frequency-domain identification. Obviously, in frequency-domain identification the curve fitting of a high-order transfer function is sensitive to the spectral resolution, the time-domain duality of which also indicates the sensitiveness of its implementation for real-time operation to the temporal resolution. As of such, the cost at implementation of compensation follows the order of compensator for a preset (PS, RO).

Figure 3b shows the appearance of  $\mu$ -manifold  $\beta(W_1, W_2)$  as Example 1 with

$$W_1(s) = \frac{3.16(s+10)}{s+100} \quad \text{and}$$

$$W_2(s) = \frac{0.316(s+100)}{s+10}$$

whose Bode magnitude plots are in Figure 3a. There is a narrow at frequency  $\omega = 31.5$  at which both  $W_1$  and  $W_2$  have magnitudes close to one. Figure 4b shows the  $\mu$ -manifold as Example 2 with high-order  $W_1(s)$  and  $W_2(s)$  plotted in Figure 4a. It is obvious that there exists a very low-order feasible loop  $S$ , even though high-order weightings boost the order of the generalized plant. Based on (P1) together with Definition 3, the longitudinal line of the feasible loop  $S$  with maximum RO keeps zero phases all the frequencies. The real line in Figure 5a is the Bode plot of the feasible loop  $S$  with maximum RO according to the  $\mu$ -manifold in Example 1. This Bode plot exposes the highness of loop's order since there must be distributed a great number of poles are zeroes in the frequency region where the magnitude is not a constant but the phase is zero. The dotted line in Figure 5a corresponds to the best curve-fitted loop with denominator and nominator being of orders up to 40. Figure 5b shows the reliability distance of the feasible loop that has a notch at the narrow of the  $\mu$ -manifold in Figure 5c, where the dotted line does not overlap the real line. Unfortunately, the dotted line does not pass through the narrow as shown in Figure 5c, which then destroys the candidacy

of the curve-fitted loop as a feasible loop. It is palpable from Figure 5 that considerable system's reliability in operation sometimes needs a compensator of high orders that is entangled with costly implementation.

There are some trade-offs among the members of the triad: PS, RO and OC discussed as follows. Firstly, for a fixed OC, the reliability distance  $d$  will be shortened if the  $\mu$ -manifold  $\beta(W_1, W_2)$  is narrowed down, that is, a higher PS accompanies a lower RO. This demonstrates that there exists a trade-off between PS and RO for a fixed OC. Secondly, for a fixed  $\mu$ -manifold, shortening the reliability distance  $d$  of a feasible loop levels the Bode-phase plot. Numerous poles and zeroes are then needed for shaping a desired Bode-magnitude curve, which results in a higher-order compensator  $K$ . That reveals there is a trade-off between RO and OC. Finally, the composition of these two trade-offs leads to a trade-off between PS and OC for a fixed RO.

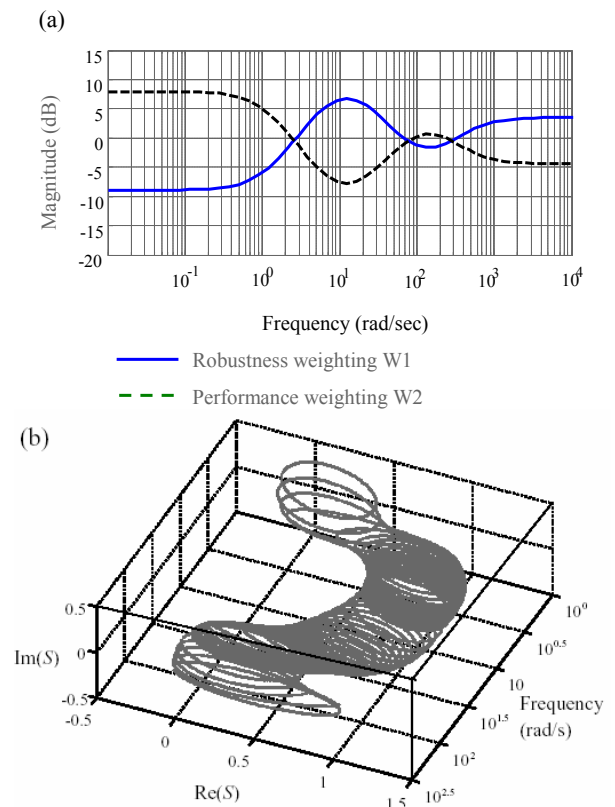


Fig.4. (a) Robustness and performance weightings of Example 2, (b) The  $\mu$ -manifold of Example2.

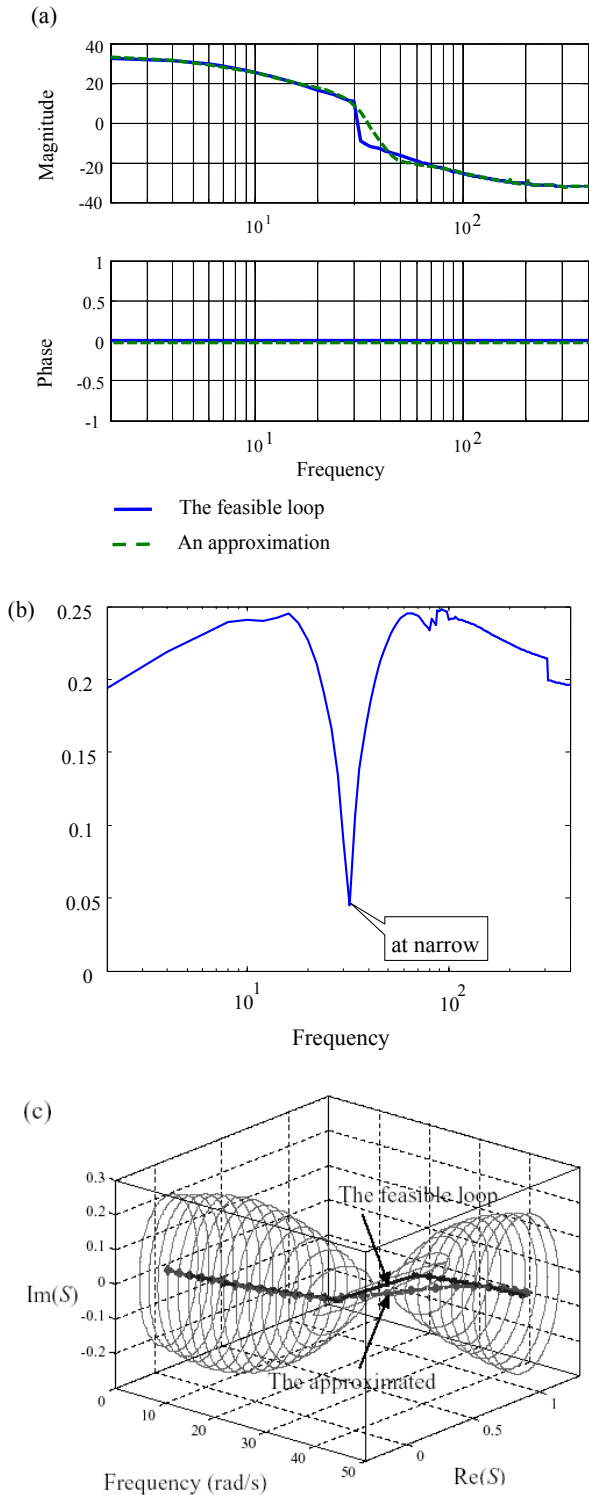
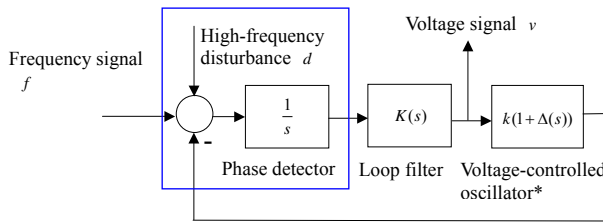


Fig.5. (a) Curve fitting of the feasible loop with maximum reliability distance, (b) The maximum reliability distance, (c) The trade-off between RO and OC.

The following steps are proposed for the semi-empirical synthesis of a custom-made compensator with a desired triad:

- (Step 1) Identify the robustness weighting  $W_1$  and then figure out a performance weighting  $W_2$  according to the  $\mu$ -plate's topology (P1)-(P8).
- (Step 2) Express the  $\mu$ -manifold  $\beta(W_1, W_2)$  in magnitude-phase coordinate for conveniently assigning desired order to the feasible loop.
- (Step 3) Plot a feasible loop  $S$  inside the  $\mu$ -manifold  $\beta(W_1, W_2)$  with a desired order.
- (Step 4) Calculate the complex numbers of the resulted compensator  $K(j\omega)$  via  $K = 1/G(1/S - 1)$  within a concerned frequency range.
- (Step 5) Identify a proper (nominator's order is not larger than denominator's order) compensator  $K(s)$  whose Bode curve is best fitted to the complex data  $K(j\omega)$ .
- (Step 6) Calculate the data-fitted feasible loop via  $S = 1/(1 + KG)$ , and check its reliability distance. If the reliability is not satisfied, then modify the feasible loop and back to Step 4.
- (Step 7) Bring the system with the compensator  $K(s)$  into test for real-time operation. Modify the feasible loop  $S$  based on the outcome response and the trade-off nature about the triad and then back to Step 3.

It is those frequency-dependent complex data  $W_1(j\omega)$  and  $W_2(j\omega)$ , instead of orders of the transfer functions  $W_1(s)$  and  $W_2(s)$ , that determine the appearance of  $\mu$ -manifold and then affect the order of feasible compensator. For a lower-ordered compensator, the robustness weighting  $W_1$  allows of enlarged order toward a better-fitted envelope of plant perturbations. Similarly, to shape a many-sided loop, we can make the performance weighting  $W_2$  rugged in Bode-magnitude plot without widening the  $\mu$ -manifold.



\* Voltage-controlled oscillator (VCO) is a common voltage-to-frequency transducer that contains a high-frequency uncertainty  $\Delta$  attached to zero-order

Fig.6. Modeling of PLL circuits served for frequency-to-voltage transducers.

## V. LOOP FILTERING OF PLL CIRCUITS – AN APPLICATION

A phase-locked-loop (PLL) circuit is widely used in industry for real-time conversion from frequency signal to voltage signal. Our modeling of a PLL circuit -made frequency-to-voltage transducer is illustrated in Figure 6.

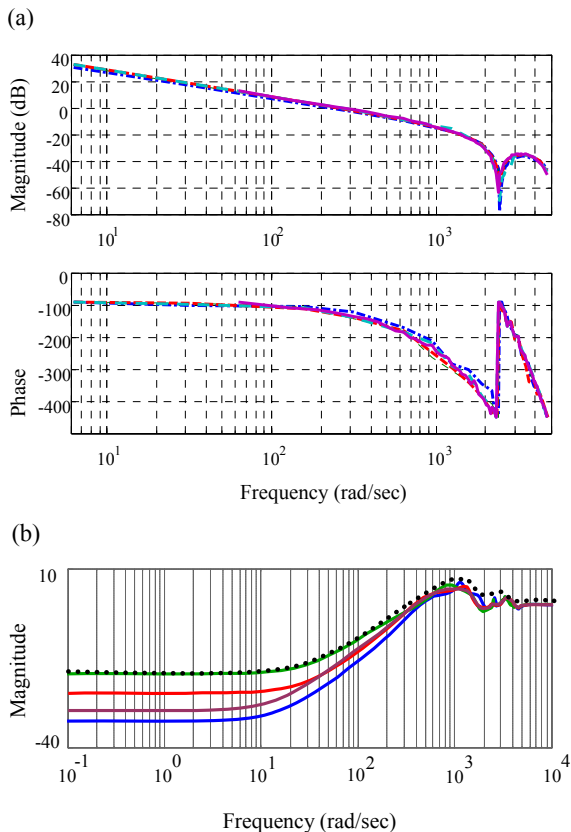


Fig.7. (a) Bode plots of PD-VCO dynamics in cd4046bc, (b) Robust weighting covering PD-VCO model perturbations.

A PLL circuit contains three main components: voltage-controlled oscillator (VCO), phase detector (PD) and loop filter (LF) [11]. The VCO is a voltage-to-frequency transducer, who converts a DC-leveled voltage in proportionality to a frequency signal. For accommodating AC-leveled voltage input to the VCO in practice, we attach a multiplicative uncertainty  $\Delta$ -VCO that is to-be-identified to the nominal dynamics of VCO, a constant  $k$ . The PD delivers the difference in voltage between the phases of its two input channels, and therefore can be modeled as a summation followed by an integration of frequency difference, as shown in Figure 6. As a steady frequency  $f$  inputs to the closed loop, the integration in the loop renders the frequency tracking a zero steady-state error. An unwanted signal, usually in high frequency, is generated from the phase comparison of PD and then filtered off through the loop filter (LF). A plant disturbance  $d$  contaminating the summation is added to model this situation. We treat the loop filtering as a feedback compensation that is to-be-synthesized for a feasible loop characterized by the triad (PS, RO, OC) under the exogenous disturbance,  $d$  and  $f$ , and the modeling uncertainty  $\Delta$ -VCO.

A pure-empirical approach based on the iteration of design-test-analysis to construct LF involves two aspects of disadvantages:

- (1) It is unable to estimate the reliability of a running frequency-to-voltage transducer. As of such, the products will have trouble with quality control or the specification of operation range.
- (2) It hunts a LF for a specific PD-VCO chip in a time-consuming process. For another type of PD-VCO chip, we have to do the hunting over again, which leads business to no profits.

Application of the  $\mu$ -topology-aided synthesis developed in Section 4 can overcomes these disadvantages.

The PD and VCO used for this application example come from a Fairchild Semiconductor Corporation manufactured chip cd4046bc. To prepare Figure 1a based on Figure 6 for introducing the  $\mu$ -topology, we need to identify the robust weighting  $W_1$  and choose

some performance weighting  $W_2$ . Here, a set of plants within a practical operation-range is firstly identified in frequency domain and then plotted in Figure 7a, where the transfer function of each plant equals that of VCO multiplied by the integrator  $1/s$ . Those Bode plots in Figure 7a correspond to the forcing responses from the sinusoidal frequency-signals, with different frequencies and magnitudes, input to the PD to the frequency-signals output from the VCO without closing the loop. Based on Figure 7a, we appoint the nominal plant  $G$  with  $G(j\omega) = (0.020265j\omega + 40.53)/j\omega$  and then calculate perturbations  $\Delta_1 W_1$  for all  $\omega$ , whose Bode-magnitudes are plotted as real lines in Figure 7b. The robustness weighting  $|W_1|$ , plotted by a dotted line, is chosen to envelop those real lines  $|\Delta_1 W_1|$  in Figure 7b so that the plants in Figure 7a belong to the set

$$(G, W_1) \equiv \{G(1 + \Delta_1 W_1) : \|\Delta_1\|_\infty \leq 1\},$$

as required in Eq. (1). Furthermore, the performance weighting  $W_2$  is chosen with the help of (P1)-(P8) as a low-pass,  $W_2(s) = (s + 800)/(s + 80)$ . This pair of weightings ( $W_1, W_2$ ) signifies that steady-state frequency tracking is guaranteed under high-frequency uncertainty.

The  $\mu$ -manifold  $\beta(W_1, W_2)$  is plotted with magnitude-phase coordinate, as shown in Figure 8a, to facilitate choosing a feasible loop with desired order. In Figure 8b, a low-order feasible loop  $S$  is chosen and its complex values  $S(j\omega)$  are marked. Complex values of the corresponding loop-filter  $K(j\omega)$  are then calculated for curve-fitting a transfer function  $K(s)$ . The best-fitted first-order compensator  $K(s)$  is found to be

$$K(s) = \frac{73.22s + 3.66 * 10^4}{s + 1987}.$$

The loop  $S(j\omega)$  with the above compensator  $K(s)$  is plotted into the  $\mu$ -manifold  $\beta(W_1, W_2)$  to check its reliability distance  $d$ , as shown in Figure 8c. In Figure 8d, it is compared with the maximum one. The found compensator is then implemented into an analog circuit in the cd40461bc chip. Figure 8e

shows a pilot run on the capability of the resulted PLL circuit served for real-time converting unsteady frequency-signal  $f$  to voltage-signal  $v$ , where  $f$  and  $v$  are defined in Figure 6.

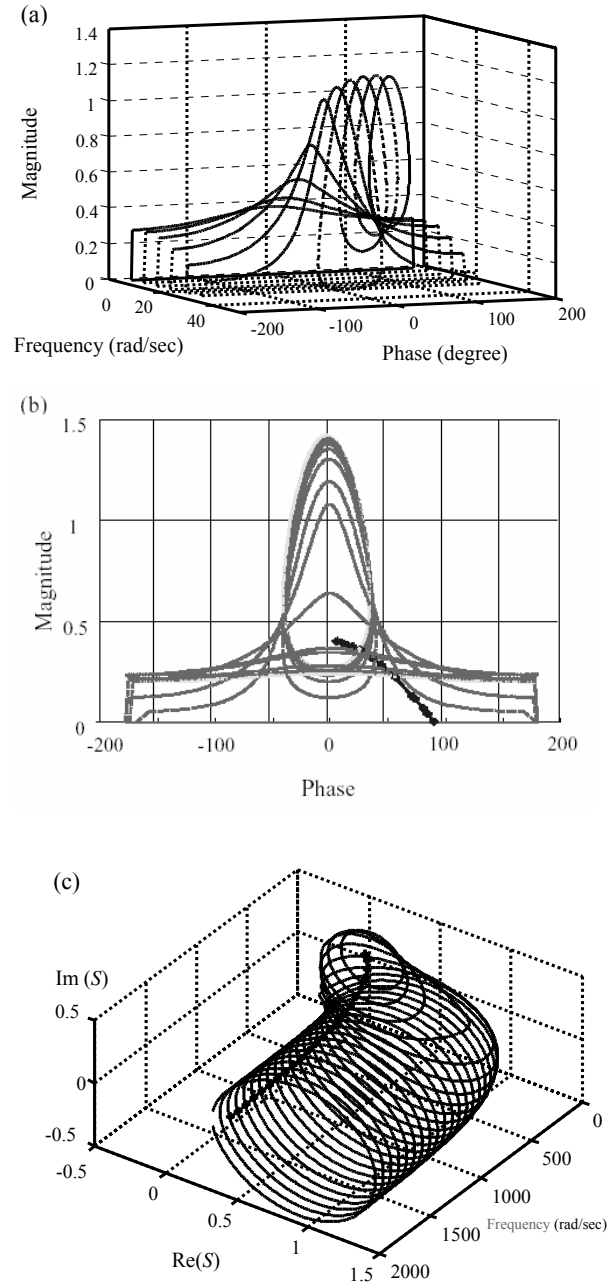


Fig.8. (a) The  $\mu$ -manifold in magnitude-phase coordinate, (b) To find a feasible loop in the  $\mu$ -manifold, (c) The chosen loop inside  $\mu$ -manifold.

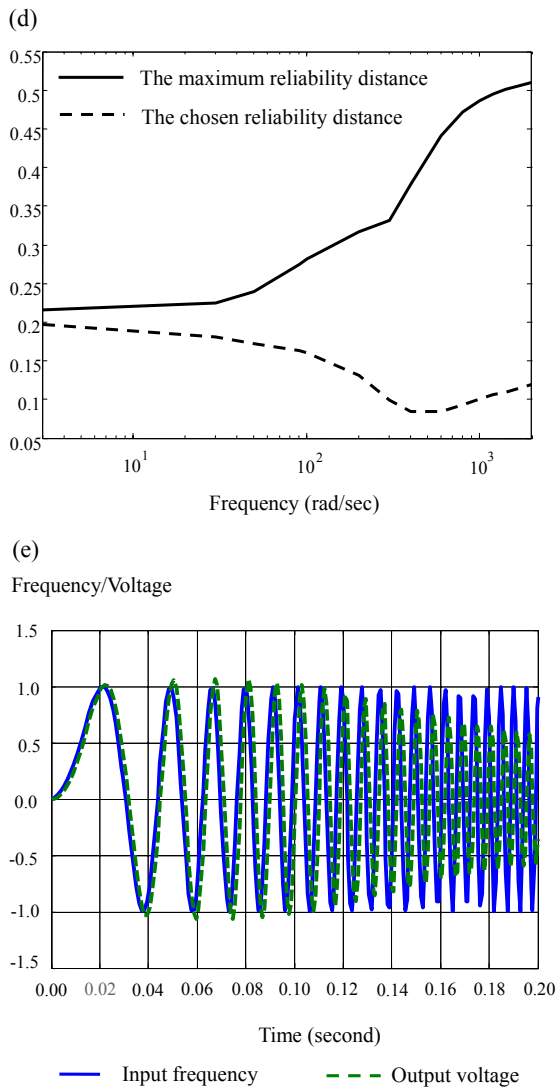


Fig.8. (d) Reliability distance of the chosen loop,  
 (e) A pilot run of the frequency-to-voltage transducer.

The compensator corresponding to the feasible loop with maximum reliability distance is plotted by real line in Figure 9a, in which a curve-fitted one with denominator-order 20 and nominator-order 17 is plotted in dotted line. They are quite close to each other within some range of frequency. However, the loop  $S$  with the curve-fitted compensator is infeasible in the region of high frequency, as shown in Figure 9b or Figure 9c. Figure 9 demonstrates that a high-order system usually has unpredictable behavior when it is operated in fast-time scale. This is a special example to emphasize the necessity of

systematic tool like the  $\mu$ -topology developed in this article for feedback compensation.

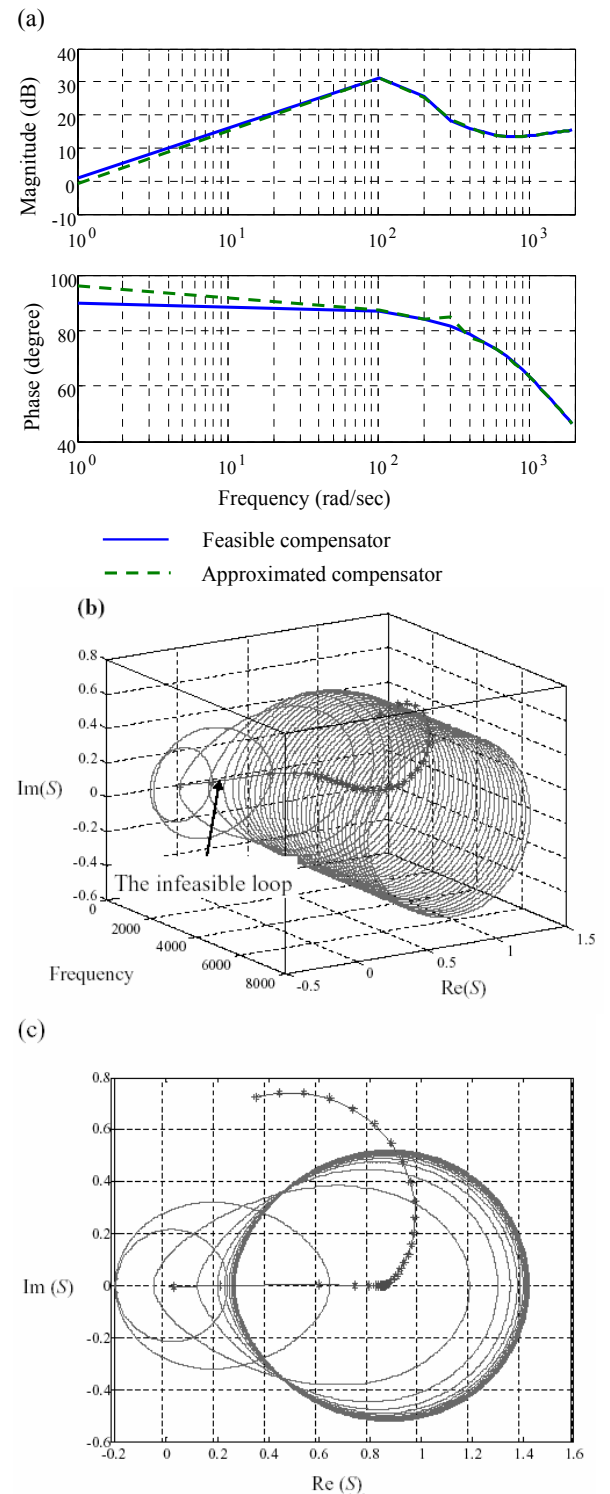


Fig.9. (a) The compensator pertaining to maximum reliability distance, (b) The sensitiveness of high-order system to fast-timed operation, (c) The projected view of Figure 9b.

## VI. SUMMARY

For the class of feedback compensations attributed to (A1)-(A5), this paper develops a topological tool to characterize a closed-loop system by a triad: performance-in-specification, reliability-in-operation and order-of-compensator. It is found that as one member of the triad is fixed, there will be a trade-off between the other two. For a fixed triad, trade-off moreover occurs between robustness and performance, between transient responses and steady responses, and also between control action and tracking error. With the aid of this topology, we further propose a semi-empirical synthesis as a systematic package for the pursuit of custom-made feedback compensators. In the last section, an instruction of putting the topology to use is provided in the application of the semi-empirical synthesis to the loop filtering in a phase-lock-loop circuit served for frequency-to-voltage transducing.

## REFERENCES

- [1] Zhou, K., Doyle, J. C., and Glover, K., Robust and Optimal Control, Prentice-Hall, Upper Saddle River, New Jersey, 1996.
- [2] Gahinet, P. and Apkarian, P., "A Linear Matrix Inequality Approach to  $H_\infty$  Control," *International Journal of Robust and Nonlinear Control*, Vol. 42, No. 4, pp. 421-448, 1994.
- [3] Scherer, C., Gahinet, P., and Chilali, M., "Multiobjective Output-feedback Control via LMI Optimization," *IEEE Transactions on Automatic Control*, Vol. 42, No. 7, pp. 896-911, 1997.
- [4] Hong, B.-S. and Ray, A., "Observer-embedded L2-Gain control," *Applied Mathematics Letters*, Vol. 14, No. 5, pp. 563-569, 2001.
- [5] Hong, B.-S., "Observer-based Parameterized LPV L2-gain Control Synthesis," *Proceedings of American Control Conference*, Anchorage, Alaska, pp. 4427-4432, 2002.
- [6] Balas, G., Doyle, J. C., Glover, K., Packard, A., and Smith, R.,  $\mu$ -Analysis and

Synthesis Toolbox for Use with Matlab, The MathWorks Inc., Natick, Maryland, 1993.

- [7] Obinata, G. and Anderson, B. D. O., Model Reduction for Control System Design, Springer-Verlag, London Limited, 2001.
- [8] Hong, B.-S., "Orthonormal Decomposition of Signals in Eigen-decomposed Linear Systems," *Mathematical and Computer Modelling*, Vol. 37, No. 12, pp. 1297-1306, 2003.
- [9] Packard, A. and Doyle, J. C., "The Complex Structured Singular Value," *Automatica*, Vol. 29, No. 1, pp. 71-109, 1993.
- [10] Hong, B.-S., Robust Control of Combustion Instabilities, Ph. D Dissertation, Department of Mechanical Engineering, The Pennsylvania State University, University Park, 1999.
- [11] Huang, Q.-Z., Robust PLL Circuit Design via Topological  $\mu$ -synthesis, Master Thesis, Department of Mechanical Engineering, National Chung Cheng University, Taiwan, 2003.

## ACKNOWLEDGEMENT

National Science Council financially supported part of this work under the grant number NSC91-2622-E-194-008-C33. The authors here express ultimate thanks.